Chapter 5

Barkhausen Noise Modelling

5.1 Existing models of hysteresis and Barkhausen noise

5.1.1 Jiles-Atherton model

Jiles and Atherton (1983) used an energy balance to model magnetic hysteresis. The energy supplied to the material by a change in applied field can be dissipated either as a change in magnetostatic energy, or as hysteresis loss.

In the absence of hysteresis, all the energy supplied would go toward modifying the magnetostatic energy. In such a case, the magnetisation would be a reversible, single-valued function of the applied field. This anhysteretic magnetisation M_{an} can be modelled as:

$$M_{an} = M_S f\{H_e\} \tag{5.1}$$

where M_S is the saturation magnetisation, $H_e = H + \alpha M$ is the Weiss mean field (Equation 3.1) and f is an arbitrary function with the properties:

$$\begin{array}{lll} f = 0 & \text{when} & H_e = 0 \\ f \to 1 & \text{when} & H_e \to \infty \end{array} \tag{5.2}$$

A modified Langevin expression (Langevin, 1905) was used to model M_{an}:

$$M_{an}\{H_e\} = M_S \left[\coth\left\{\frac{H_e}{a}\right\} - \left(\frac{a}{H_e}\right) \right] \tag{5.3}$$

where a is a parameter with units of field.

The energy supplied E_{supp} can therefore be expressed in terms of M_{an}:

$$E_{supp} = \mu_0 \int M_{an}\{H\}\mathrm{d}H \tag{5.4}$$

Hysteresis loss was attributed to domain wall pinning by sites distributed at random, all of which had the same pinning energy for 180° walls, $< \varepsilon_\pi >$. For other domain wall angles θ, the pinning energy $< \varepsilon_{pin} >$ is:

$$< \varepsilon_{pin} >= \frac{1}{2} < \varepsilon_\pi > (1 - \cos\theta) \tag{5.5}$$

For an average pinning site density per unit volume n, the total energy dissipated against pinning E_{pin} when a domain wall of area A sweeps out a distance x between domains at an angle θ to one another is:

$$E_{pin}\{x\} = \int_0^x \frac{n < \varepsilon_{pin} >}{2m}(1 - \cos\theta)A\mathrm{d}x \tag{5.6}$$

where m is the magnetic moment of a typical domain. This gives a net change in magnetisation $\mathrm{d}M$:

$$\mathrm{d}M = m(1 - \cos\theta)A\mathrm{d}x \tag{5.7}$$

Hence E_{pin} can be expressed in terms of M:

$$E_{pin}\{M\} = \frac{n < \varepsilon_{pin} >}{2m} \int_0^M \mathrm{d}M \tag{5.8}$$

The constant $n < \varepsilon_{pin} > /2m$ was termed the pinning parameter k.
Equating E_{supp} with the sum of E_{pin} and the magnetostatic energy due to the change in magnetisation $\mathrm{d}M$ gives:

$$\frac{\mathrm{d}M}{\mathrm{d}H} = \frac{M_{an}\{H\} - M\{H\}}{k} \tag{5.9}$$

A subsequent modification allowed for reversible magnetisation M_{rev}, assuming wall-bowing in the direction tending to reduce the difference between the actual magnetisation M and M_{an}:

$$M_{rev} = c(M_{an} - M) \tag{5.10}$$

where c is a constant. The final equation is then given by:

$$\frac{\mathrm{d}M}{\mathrm{d}H} = \frac{M_{an}(H) - M_{irr}(H)}{(k\delta/\mu_0) - \alpha(M_{an}(H) - M_{irr}(H))} + c\left(\frac{\mathrm{d}M_{an}}{\mathrm{d}H} - \frac{\mathrm{d}M}{\mathrm{d}H}\right) \tag{5.11}$$

where M_{irr} is the irreversible component of magnetisation and δ is a parameter inserted to account for the direction of field increase:

$$\begin{aligned} \delta &= +1 \text{ for } \mathrm{d}H/\mathrm{d}t > 0 \\ \delta &= -1 \text{ for } \mathrm{d}H/\mathrm{d}t < 0 \end{aligned} \tag{5.12}$$

Hysteresis can therefore be expressed in terms of five constants: α, a, M_S, c and k. Jiles and Atherton later modified k so that it had the same dimensions as H_C:

$$k = \frac{n < \varepsilon_{pin} >}{2m\mu_0} \tag{5.13}$$

Extensions have been made to this model to allow the modelling of minor loops (Jiles and Atherton, 1984; Carpenter, 1991), and the effects of magnetocrystalline anisotropy (Ramesh *et al.*, 1996, 1997) and crystal texture (Shi *et al.*, 1998). Methodologies for the extraction of modelling parameters from experimental data have also been developed (*e.g.* Jiles *et al.*, 1992; Del Moral Hernandez *et al.*, 2000).

5.1.2 Preisach model

An earlier model by Preisach (1935) considered a magnetic material as an assemblage of particles, each of which could be in one of two magnetisation states. The particle switches between these states at particular field values. If the particle were isolated, its hysteresis loop would be symmetrical, but interactions with other particles with different switching fields shifts the loop along the H axis. The overall behaviour of the material is modelled using a Preisach distribution function, which is a statistical representation of the number of domains switching their states as the applied field is changed. This model is widely used for the magnetic properties of recording media (Jiles, 1998) and has been the subject of many developments and modifications since its introduction.

5.1.3 Equivalence of models and relationship to microstructure

Dupré *et al.* (1999) identified the relationships between modelling parameters in the Jiles-Atherton and Preisach models. Pasquale *et al.* (1999) also demonstrated that the two formulations were equivalent and found simple relationships between the Jiles-Atherton parameter k and the grain size in nonoriented silicon steel, and between k and other material parameters in a metallic glass. Further work has demonstrated that the Jiles-Atherton parameters k and a are affected by the grain diameter d_g and dislocation density ρ_d:

$$\begin{aligned} k = &\quad k_0 \left(G_1 + \tfrac{G_2}{d_g}\right) \sqrt{\rho_d} \\ a = &\quad a_0 \left(G_1 + \tfrac{G_2}{d_g}\right) \sqrt{\rho_d} \end{aligned} \tag{5.14}$$

where k_0, a_0, G_1 and G_2 are constants (Sablik, 2001). The rationale behind this formulation was that k, being a measure of the hysteresis loop width, was proportional to the coercive field, which was found from a survey of previous work to depend on the reciprocal of the grain size and the square root of dislocation density. The parameter a was found by Sablik and Jiles (1993) to be proportional to the domain density in the demagnetised state, which should be proportional to the pinning site density and hence to k. Numerical experiments, using values obtained from previous experimental work and the dependencies in Equation 5.14, were performed by Dupré *et al.* (2002) to investigate the variation of the Preisach model parameters on dislocation density and grain size. It appears that, so far, there has been no work on the effects of particles on modelling parameters.

5.1.4 Alessandro, Beatrice, Bertotti and Montorsi (ABBM) model

Alessandro *et al.* (1990a) developed a model for BN based on stochastic fluctuations in the coercivity, initially considering a single, planar 180° domain wall. Williams, Shockley and Kittel (1950) showed that, for macroscopic domain wall movement, the wall velocity v was proportional to the difference

between the field acting on the wall H and the coercive field H_C:

$$kv = H - H_C \tag{5.15}$$

where k is a constant characterising eddy current damping. Alessandro *et al.* assumed that this relationship was also valid for local fluctuations of H_C on a microstructural scale.

The rate of change of magnetic flux $\dot{\Phi}$ is related to the domain wall velocity v by the equation:

$$\dot{\Phi} = 2\mu_0 M_S \mathrm{d}v \tag{5.16}$$

where M_S is the saturation magnetisation. Thus,

$$\sigma G \dot{\Phi} = H - H_C \tag{5.17}$$

where σ is the electrical conductivity and G is a dimensionless coefficient.

The correlation length ξ characterises the range over which a domain wall interacts with a perturbation. The H_C fluctuations were modelled by considering H_C as a random function of domain wall position, and hence of Φ:

$$\frac{\mathrm{d}H_C}{\mathrm{d}\Phi} + \frac{H_C - < H_C >}{\xi} = \frac{\mathrm{d}W}{\mathrm{d}\Phi} \tag{5.18}$$

where

$$< \mathrm{d}W >= 0, < |\mathrm{d}W|^2 >= 2A\mathrm{d}\Phi \tag{5.19}$$

and A is an unknown constant. The term W represents noise, leading to stochastic fluctuations in H_C, and A characterises the amplitude of these fluctuations.

The magnetic field H experienced by the domain wall depends on both the applied field and the demagnetising field H_d. Because of the difficulty of determining H_d exactly, Alessandro *et al.* restricted the model to regions in which the differential permeability was constant.

Using this basis, models for the pulse amplitude distribution and the power spectrum (*i.e.* Fourier transform) of BN were obtained by applying the theory developed for a single domain wall to the movement of an assemblage of walls. These models agreed reasonably well with experimental measurements of BN from nonoriented Fe-3 wt. % Si within the constant differential permeability regime (Alessandro *et al.*, 1990b).

5.1.5 Extensions to ABBM

Potential energy model

McMichael *et al.* (1993) used ABBM concepts in a BN model for the whole hysteresis loop. Domain walls were assumed to be rigid and planar. The energy per unit area E of a domain wall element under an applied field H is given by:

$$E = -2M_S Hx + E_{dw}\{x\} \tag{5.20}$$

where x is the domain wall position measured normal to the wall area, M_S is the saturation magnetisation, and $E_{dw}\{x\}$ is the domain wall energy per unit area as a function of its position. The force F on the wall is the derivative of its energy with respect to position:

$$F = \frac{\partial E}{\partial x} = 2M_S H - \frac{\partial E_{dw}\{x\}}{\partial x} \tag{5.21}$$

Normalised variables $f = F/2M_S$ and $H_C\{x\} = (1/2M_S)(\partial E_{dw}\{x\}/\partial x)$ were used, and the domain wall was considered to move in a positive direction for $f > 0$ $[H > H_C\{x\}]$ and in a negative direction for $f < 0$ $[H < H_C\{x\}]$. For $f = 0$ the wall was in a position of equilibrium, but this was only stable for $\mathrm{d}H_C/\mathrm{d}x > 0$, *i.e.* a minimum-energy position.

The combined effect of movements of N domain walls contributes to the magnetisation M:

$$M = \frac{1}{N}\sum_{i=1}^{N} A_i x_i \tag{5.22}$$

where A_i and x_i are the area and position of the ith wall element.

The fluctuations in $h_{ci}\{x_i\}$ are modelled in a similar form to the ABBM model (Equation 5.18):

$$\frac{\mathrm{d}h_{ci}}{\mathrm{d}x_i} = \frac{h_{ci}}{\xi} + \frac{\mathrm{d}W}{\mathrm{d}x_i} \tag{5.23}$$

where, as in Equation 5.18, ξ represents a correlation length and W a noise term with $< \mathrm{d}W_i >= 0, < |\mathrm{d}W_i|^2 >= 2B\mathrm{d}x_i$, B characterising the size of fluctuations in h_{ci}. In this model, the field H is obtained from:

$$H = H_a - N_d M \tag{5.24}$$

where M is magnetisation given by Equation 5.22, H_a is the applied field and N_d is the demagnetising factor.

Combination with Jiles-Atherton

Jiles *et al.* (1993) started, instead, from the rate of change of magnetisation $\dot{M}$, which was kept constant in the original ABBM model:

$$\dot{M} = \left(\frac{\mathrm{d}M}{\mathrm{d}H}\right)\left(\frac{\mathrm{d}H}{\mathrm{d}t}\right) = \chi'\dot{H} \tag{5.25}$$

where χ' is the differential susceptibility.

The BN jump sum M_{JS} is the product of the number of BN events N and average event size $< M_{disc} >$. The rate of change of M_{JS} with time was assumed to be proportional to $\dot{M}$:

$$\frac{\mathrm{d}M_{JS}}{\mathrm{d}t} \propto \chi'\dot{H} \tag{5.26}$$

Assuming that the average BN jump size $< M_{disc} >$ remains constant throughout, and expressing the number of events per unit change of magnetisation as $N'\{t_n\} = \mathrm{d}N\{t_n\}/\mathrm{d}M$, the rate of change of M_{JS} with time was modelled as:

$$\frac{\mathrm{d}M_{JS}\{t_n\}}{\mathrm{d}t} \propto \chi'\left[N'\{t_{n-1}\} + \delta_{rand}\sqrt{N'\{t_{n-1}\}}\right] \tag{5.27}$$

where δ_{rand} is a random number between -1 and $+1$. Predictions of BN signals were made by combining this model with the Jiles-Atherton model

predictions of χ'. In a later modification, Lee *et al.* (2001) proposed that the anhysteretic differential susceptibility $\mathrm{d}M_{an}/\mathrm{d}H$ should be used instead of $\mathrm{d}M/\mathrm{d}H$.

Variations in average coercive field

In Equation 5.18, the average coercive field $< H_C >$ is constant. Clatterbuck *et al.* (2000) proposed that the restriction of ABBM to constant applied fields could be relieved by varying this average as a function of position on the hysteresis loop. The magnetisation then sweeps out a hysteresis loop whose behaviour, over a large number of cycles, is close to the average behaviour, but whose fine structure varies from one cycle to the next because of the random noise component. By varying the parameters ξ and A, this model could be fitted well to experimental BN data from nickel.

5.1.6 Relationships between ABBM parameters and real data

Recent work has investigated relationships between fitting parameters and microstructural data. Lee *et al.* (2001) measured hysteresis loops and BN from Fe-0.05 wt. % C. The Jiles-Atherton model parameters were obtained by fitting the hysteresis loop, and substituted into an ABBM-type model. This allowed good replication of the noise peak position by the model.

Ferritic-pearlitic steels with a variety of carbon contents have also been investigated in the same way (Lo *et al.*, 2002). By adjusting the model parameters ξ and A, it was found that ξ had a strong effect on the simulated pulse height distributions, while A influenced them only weakly. A was held constant and ξ fitted to the experimental data, giving a relationship:

$$\xi = C_1 V_F d_F + C_2 V_P d_P \tag{5.28}$$

where V_F and V_P are the volume fractions of ferrite and pearlite, and D_F and D_P the ferrite and pearlite grain sizes, respectively, and C_1 and C_2 are constants. This simple combination of ferrite and pearlite effects is similar to Equation 4.1.

According to this relationship, the range ξ over which a domain wall interacts with a pinning site depends on the sizes of the grains. Lo *et al.* state that the interaction range is related to the displacement of the wall between pinning sites. There seems to have been a subtle change in the meaning of the term ξ since the original paper by Alessandro *et al.* (1990a); it was then regarded as the range of influence of a pinning site, but Lo *et al.* consider it more as a 'mean free path' between sites. These differences can be reconciled if it is considered that the wall is always within the range of influence of one site or another. This may well be the case in a material with a high defect density such as ferritic-pearlitic steel.

5.1.7 Microstructure-based modelling

Sakamoto *et al.* (1987) modelled the effect of grain size and particle distributions on the RMS Barkhausen noise. It was assumed that all BN pulses had the same duration 2σ and that the time interval between successive pulses τ was also constant. The RMS noise was modelled as:

$$\mathrm{RMS} = C_R \cdot \frac{\tau^2}{\sigma^2} \tag{5.29}$$

where

$$C_R = \frac{1}{8\sqrt{2\pi}H_{max}} \left(\frac{\mathrm{d}H}{\mathrm{d}t}\right) (N \cdot \Delta\Phi) \tag{5.30}$$

and H_{max}, $\mathrm{d}H/\mathrm{d}t$, N and $\Delta\Phi$ are the maximum applied field, the rate of change of field, the number of pulses per unit cross-sectional area and the magnetic flux change respectively.

Expressions for the RMS noise in terms of the microstructure were derived by assuming that the majority of noise originated from domain nucleation and growth.

Grain boundaries

Assuming that the nucleation of a domain wall at a grain boundary, and its propagation across to the opposite side of the grain, produced a single noise pulse of duration 2σ,

$$\sigma = d_g/2\bar{v} \tag{5.31}$$

where d_g is the grain diameter and $\bar{v}$ the average wall velocity.

By combining previous results from Döring (1938), Williams (1950), Nagashima (1959), Bloor and Martin (1959) and Carey (1960), an expression for the RMS voltage was derived in terms of grain size d_g and a grain-size-independent term C_g:

$$\text{RMS} = C_g d_g^{-1/2} \tag{5.32}$$

Particle distributions

In the case of a ferrite microstructure containing cementite particles, after nucleating at the grain boundaries, the domain walls would encounter the particles and be pinned. For a pulse of duration 2σ, in this case:

$$\sigma = \frac{\bar{s}}{2C_v H_p} \tag{5.33}$$

where $\bar{s}$ is the domain wall mean free path, C_v is a proportionality constant and H_p is the pinning field. $\bar{s}$ was approximated to $d_p/\alpha^{1/3}$, where d_p is the cementite particle diameter and α the volume fraction of particles. H_p was obtained from an expression due to Kersten (1943):

$$H_p = 2.5 \left(\frac{K}{\mu_0 M_S}\right) \left(\frac{\delta}{d_p}\right) \alpha^{2/3} \tag{5.34}$$

where δ is the domain wall width and K the anisotropy constant.

The number of pulses N was equated to the number of cementite particles per unit area, $6\alpha/\pi d_p^3$, giving a value for τ:

$$\tau = \frac{\pi t_{total}}{6} \frac{d_p^3}{\alpha} \tag{5.35}$$

so that the RMS voltage is given by:

$$\text{RMS} = C_p d_p^2 \tag{5.36}$$

where, as above, the term C_p is independent of the particle diameter d_p.

Good agreement with experiment was obtained for the dependence of the RMS noise on d_g in ferrite without cementite. In an alloy containing particles, the experimental data agreed with Equation 5.36 for particles smaller than 1 μm in diameter, but broke down when they were larger than this. It is likely that this is due to the dominance of the magnetostatic pinning effect and the formation of spikes when particles are larger (§ 3.3.1).

5.1.8 Models for power plant steels

Domain nucleation and growth

Kameda and Ranjan (1987a) considered that the magnetic BN signal intensity was proportional to $\mathrm{d}B/\mathrm{d}t$ and the effective surface skin area A from which noise originated. B was expressed as:

$$B = \lambda \left[\beta_n N_n + \left(\frac{\bar{s}}{\delta_w} \right) N_g \right] \tag{5.37}$$

where λ is a coefficient related to the atomic magnetic moment, β_n a coefficient related to the spike shape of nucleated domains, N_n the density of nucleated walls, $\bar{s}$ the average displacement of growing domains, δ_w the domain wall thickness and N_g the density of propagating domain walls. The first term describes domain nucleation, and the second, domain growth.

Kameda and Ranjan predicted that $\mathrm{d}N_n/\mathrm{d}H$ would be a maximum as the field was reduced from saturation and the nucleation of domains allowed a reduction in magnetostatic energy. $\mathrm{d}N_g/\mathrm{d}H$ was believed to have a more complex form, with two maxima and two minima, and a smaller maximum amplitude than $\mathrm{d}N_n/\mathrm{d}H$. They considered that the BN behaviour would be dominated by nucleation when the number of defects was large, for example in a power plant steel after quenching. Reducing the density of defects would give a larger mean free path $\bar{s}$, allowing domain growth to become significant. This interpretation was used to explain the change from a single to a double peak on tempering martensitic steel.

Moorthy *et al.* interpretation

The alternative interpretation of power plant steel BN data, by Moorthy *et al.* (1997b, 1998, 2000) was introduced in § 4.7.3. Pinning sites due to grain boundaries were considered to have a distribution of strengths with a width ΔH_{gb} and average value $\bar{H}_{gb}$, and pinning sites due to carbide particles could likewise be described by ΔH_{cp} and $\bar{H}_{cp}$. Magnetisation was described as a two-stage process: firstly, the domain walls nucleated at, and became unpinned from, the grain boundaries and were pinned by the carbides, and secondly, they were unpinned from the carbides. The two sets of unpinning events were each associated with a peak in BN emission.

5.1.9 Summary

It has been seen that there are several modelling strategies for magnetic hysteresis and BN:

1. Use of an energy balance to model hysteresis, with a single parameter to characterise pinning strength.
2. Preisach-type models using distributions of subunits, each of which can adopt one of two states.
3. Models based on stochastic fluctuations in local coercive field, characterised by their amplitude and interaction range.
4. Quantitative microstructural interpretations based on the effect of feature spacing on jump sizes.
5. Considerations of the probability of domain nucleation and growth.
6. Qualitative microstructural interpretations based on distributions of pinning site strengths due to grain boundaries and carbides.

If, as is suggested by Moorthy *et al.*, both grain boundary and carbide particle pinning sites play a part in the overall BN behaviour, it is possible that models of types 1 and 3 will not be able to accommodate the complexity

of the problem without the introduction of, for example, a second k parameter in the Jiles-Atherton model or two distributions of H_C fluctuations in ABBM-type models. The Sakamoto *et al.* model (4) considers both kinds of sites, but these were used to model the overall RMS noise rather than the variation of the BN voltage with H. Kameda and Ranjan (5) considered the effect of pinning site densities on mean free path, and Moorthy *et al.* (6) introduced the idea of distributions of pinning site strengths. These two concepts were used to develop a new model of the dependence of BN voltage on H in a steel containing two types of pinning sites.

5.2 A new model for BN in power plant steels

This model considers statistical distributions of pinning site strengths from two types of microstructural features, and their combined effect on the number of BN events and the domain wall mean free path as H varies.

Initially, domain walls are pinned in place by both grain boundaries and carbides. At a certain value of applied field, those pinned by grain boundaries are released, but the carbide-pinned domain walls remain in place until the field has increased sufficiently for them to escape. This model is slightly different from that of Moorthy *et al.*, in which the walls are initially considered to be pinned only by grain boundaries.

The distance moved by a domain wall after unpinning, and the resulting change in magnetisation, depend on the spacing of domain wall obstacles. Pinning sites which act as obstacles at low applied fields may easily be bypassed at higher fields, so that they would no longer act as effective pinning sites. This new model therefore considers the domain wall mean free path as a function of applied field, rather than adopting a constant value as has been used in most previous interpretations apart from the work of Kameda and Ranjan (1987a).

5.3 Assumptions

It is assumed that all domain walls are planar and of Type-II character. BN events are due solely to domain wall motion, and the number of domain walls remains constant, within the applied field range of interest. The domain wall surface area also remains the same throughout, and domain walls do not interact with one another. In essence, it is assumed, as in the ABBM model, that the ensemble of domain walls behaves in exactly the same way as would a single wall. The domain walls are assumed always to move in discrete jumps rather than continuously. Their motion is assumed to be rapid compared to the rate of change of field with time.

Fluctuations in the coercive field or potential energy originate only from microstructural features, which are distributed evenly in space. The strength

of these pinning sites is characterised not by a constant but by a statistical distribution. It is assumed for the sake of simplicity that there is no energetic interaction between pinning sites.

Based on previous experimental observations, it is proposed that the number and type of pinning sites which are actively able to obstruct domain walls varies with the applied field. The field required to overcome a pinning site is determined by the local coercive, or pinning, field. If the field experienced by the domain walls is H, pinning sites with $H_C < H$ can be overcome, and only those with $H_C \geq H$ will resist wall motion.

The actual field experienced by the domain wall differs from the applied field by an amount depending on the magnetisation and the demagnetising factor. Many previous models have relied on the assumption that the BN signal amplitude is proportional to the rate of change of magnetisation $\mathrm{d}M/\mathrm{d}t$ or induction $\mathrm{d}B/\mathrm{d}t$. If this relationship were to be used here then it would be possible to estimate the demagnetising field. However, it has been shown experimentally that this proportionality does not always hold (Kim *et al.*, 1992) and that the regime of its applicability is complex, depending on the microstructural condition and the applied field amplitude. It was therefore decided to avoid using this relationship.

A possible solution to this problem of demagnetising fields would be to obtain the magnetisation as a function of applied field from the Jiles-Atherton or Preisach model, as used when fitting ABBM-type models, and use this to modify the field value for the new model. However, the published data sets used for the fitting did not include hysteresis measurements.

It was considered that, for the initial development of the model, demagnetising fields should be assumed not to have a significant effect on the behaviour of the domain walls. Since BN measurement geometry is designed to minimise demagnetising and stray fields, this assumption may be reasonable. Modifications to include a demagnetising factor could be made if the model showed promise.

5.4 Origin of the noise

A domain wall of surface area $\mathbf{A}_w$, moving a distance $\mathbf{l_w}$ and sweeping out a volume $(\mathbf{A}_w.\delta\mathbf{l_w})$, causes a change in magnetisation $\delta\mathbf{m}$:

$$\delta\mathbf{m} = \beta(\mathbf{A}_w.\delta\mathbf{l_w}) \tag{5.38}$$

where β depends on the angle between the magnetisation of adjacent domains and the atomic magnetic moment (Saquet *et al.*, 1999). If it is assumed that the domain walls always move in a direction parallel to the normal of the domain wall plane, then the expression $(\mathbf{S}.\delta\mathbf{l})$ reduces to $S \cdot \delta l$. The total change in magnetisation $\delta M\{H\}$ at a certain field H is given by the product of the number of domain wall movement events at field H, $N\{H\}$ and the vector sum of all the individual changes $\delta\mathbf{m}$. Assuming that all the domain walls involved are Type-II (180°), β is constant, and Equation 5.38 reduces to:

$$\delta M\{H\} \propto N\{H\} < l > \{H\} \tag{5.39}$$

where $< l > \{H\}$ is the average domain wall displacement (mean free path) at field H.

The electric field amplitude E_0 induced by this change in magnetisation is given by the rate of change of magnetisation with time. For a discrete change in magnetisation, this is given by:

$$E_0 = \frac{\delta M}{\delta t} \tag{5.40}$$

where δt is the time interval over which the change occurs. As mentioned above, it is assumed that the domain walls move rapidly enough that the change in magnetisation $\delta M\{H\}$ occurs immediately the field is changed, and does not depend on the rate of change of field.

The noise voltage V measured by the pickup coil depends on the noise frequency, with higher-frequency noise experiencing more signal attenuation (Saquet *et al.*, 1999). However, for low-frequency noise, the measured voltage can be considered to be proportional to E_0. For simplicity, therefore, it is

assumed that the frequency f is low enough to avoid attenuation and to allow a simple proportionality between the change of magnetisation and the measured pulse size:

$$V \propto N\{H\} < l > \{H\} \tag{5.41}$$

This is the simple relationship 'Noise amplitude = number of events × mean free path' which is sometimes used to interpret BN signals in the literature, but it is only truly valid in a limited range of circumstances.

5.5 Construction of the statistical model

5.5.1 Distribution of pinning sites

Initially, it was assumed that the number of pinning sites per unit volume with pinning strength S, $n\{S\}$, follows a normal distribution with mean value $< S >$ and standard deviation ΔS. The total number of pinning points per unit volume was A. Thus:

$$n\{S\} = \frac{A}{\Delta S\sqrt{2\pi}} \cdot \exp\left\{-\frac{1}{2}\left(\frac{S- < S >}{\Delta S}\right)^2\right\} \tag{5.42}$$

5.5.2 Impediments to domain wall motion

When the material experiences a magnetic field H, pinning sites with pinning strength $S \geq H$ are able to impede domain wall motion. These sites will be referred to as 'active sites'.

The number of active sites per unit volume $N\{H\}$ is given by the integral of $n\{S\}$ with respect to S from H to infinity:

$$N\{H\} = \int_H^\infty n\{S\}\mathrm{d}S \tag{5.43}$$

Thus:

$$N\{H\} = \frac{A}{2}\ \mathrm{erfc}\left\{\frac{H- < S >}{\Delta S\sqrt{2}}\right\} \tag{5.44}$$

5.5.3 Mean free path of domain walls

In order to estimate the mean free path, it is necessary to make an assumption about the arrangement of the active pinning sites. A suitably basic first approximation is to consider all the pinning sites as points arranged in a simple cubic lattice, with one site per cube of side l, where $l = l\{H\}$:

$$l\{H\} = \left(\frac{1}{N\{H\}}\right)^{\frac{1}{3}} \tag{5.45}$$

The mean free path of domain walls travelling through the material can be approximated to $l\{H\}$:

$$< l > \{H\} = l\{H\} \tag{5.46}$$

The assumptions made to derive this expression are crude, taking no account of the planar nature of grain boundaries, variations in carbide diameter, or phenomena such as the preferential nucleation of carbides at grain boundaries, but subsequent refinements could be made if the model showed promise.

5.5.4 Number of Barkhausen events occurring

Assuming for simplicity that there are no demagnetising fields, the field H experienced by the material is equal to the applied field. The number of Barkhausen events occurring due to domain wall unpinning at applied field H is equal to the number of pinning sites of strength $S = H$.

This is obtained from Equation 5.42:

$$n\{H\} = \frac{A}{\Delta S\sqrt{2\pi}} \cdot \exp\left\{-\frac{1}{2}\left(\frac{H - < S >}{\Delta S}\right)^2\right\} \tag{5.47}$$

5.5.5 Barkhausen amplitude

Adopting the assumption that the RMS voltage $V\{H\}$ at field H is proportional to the number of Barkhausen events $n\{H\}$ multiplied by the mean free path $< l > \{H\}$:

$$V\{H\} = C \cdot n\{H\} \cdot < l > \{H\} \tag{5.48}$$

where C is a constant, gives:

$$V\{H\} = C \cdot \frac{A}{\Delta S\sqrt{2\pi}} \cdot \exp\left\{-\frac{1}{2}\left(\frac{H - < S >}{\Delta S}\right)^2\right\} \cdot \left[\frac{A}{2}\ \mathrm{erfc}\left\{\frac{H - < S >}{\Delta S\sqrt{2}}\right\}\right]^{-\frac{1}{3}} \tag{5.49}$$

5.5.6 Multiple distributions of pinning points

Different types of pinning site can be modelled by introducing more than one distribution, with different constant terms for each:

$$n_i\{S\} = A_i \cdot \exp\left\{-\left(\frac{S - < S >_i}{(\Delta S)_i}\right)^2\right\} \tag{5.50}$$

The overall number of pinning sites with a pinning strength greater than H is now given by:

$$N\{H\} = \sum_{i=1}^{m} \int_H^\infty n_i\{S\}\mathrm{d}S \tag{5.51}$$

where m is the total number of pinning site distributions.

Thus:

$$N\{H\} = \sum_{i=1}^{m} \frac{A_i\sqrt{\pi}}{2(\Delta S)_i} \cdot \mathrm{erfc}\left\{\frac{H - < S >_i}{(\Delta S)_i}\right\} \tag{5.52}$$

The relation $V\{H\} = C \cdot n\{H\} \cdot < l > \{H\}$ (Equation 5.48) should still apply as long as there are no preferential orientations of particular types of sites; hence:

$$V\{H\} = C \cdot \sum_{i=1}^{m} \frac{A_i\sqrt{\pi}}{2(\Delta S)_i} \cdot \mathrm{erfc}\left\{\frac{H - < S >_i}{(\Delta S)_i}\right\} \tag{5.53}$$

Plots of this function for $m = 2$ were able to replicate single-peak, shoulder and double-peak behaviour when appropriate values of the parameters A_i, $< S >_i$ and ΔS_i were selected. An example is shown in Figure 5.1. This

first attempt at modelling, using two normal distributions, is referred to as Model 1.

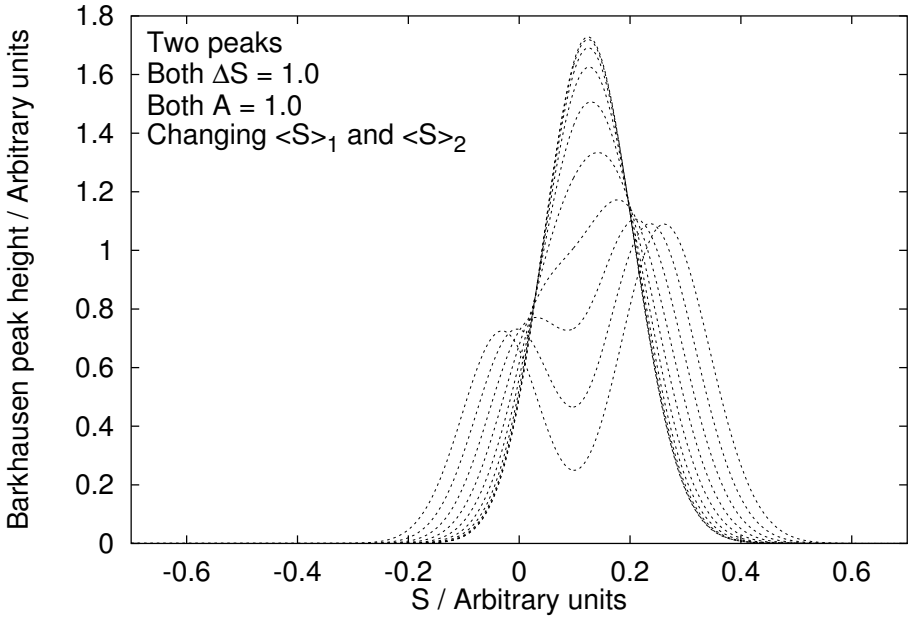

Figure 5.1: Transition between single- and double-peak behaviour

5.6 Log-normal model

In the real experimental data sets shown in Figure 5.2, the lower-field peak appears asymmetric. A modified model, in which the pinning site strengths contributing to this peak follow a log-normal distribution (Mihram, 1972), was therefore proposed:

$$n\{S\} = \begin{cases} \frac{A}{S\Delta x\sqrt{2\pi}} \cdot \exp\left\{-\frac{1}{2}\left(\frac{\ln(S-S_b)-<x>}{\Delta x}\right)^2\right\} & S > 0 \\ 0 & S \leq 0 \end{cases} \tag{5.54}$$

where $< x >$ and Δx are the mean value and the standard deviation of $\ln(S - S_b)$ respectively, and S_b is the field at which the first unpinning events due to this distribution occur.

This gives an integrated value from H to infinity of:

$$N\{H\} = \begin{cases} \frac{A}{2} \cdot \mathrm{erfc}\left\{\frac{\ln(H-S_b)-<x>}{\Delta x\sqrt{2}}\right\} & S > 0 \\ 0 & S \leq 0 \end{cases} \tag{5.55}$$

If, as suggested by Moorthy *et al.*, the pinning strengths contributing to the first peak are related to grain size, a log-normal distribution would be a reasonable assumption, since this is the approximate distribution found in experiment (Okazaki and Conrad, 1972; Rhines and Patterson, 1982; Pande, 1987, reported in Krill and Chen, 2002).

The second peak, as before, is modelled as a normal distribution. The overall model is constructed in the same way as above, and referred to as Model 2.

5.7 Summary of model equations

Model 1

$$\begin{aligned} n_1\{S\} = &\quad A_1 \cdot \exp\left\{-\left(\frac{S-<S>_1}{(\Delta S)_1}\right)^2\right\} \\ n_2\{S\} = &\quad A_2 \cdot \exp\left\{-\left(\frac{S-<S>_2}{(\Delta S)_2}\right)^2\right\} \end{aligned} \tag{5.56}$$

Model 2

$$\begin{aligned} n_1\{S\} = &\quad \begin{cases} \frac{A_1}{S\Delta x\sqrt{2\pi}} \cdot \exp\left\{-\frac{1}{2}(\frac{\ln(S-S_b)-<x>}{\Delta x})^2\right\} & S > 0 \\ 0 & S \leq 0 \end{cases} \\ n_2\{S\} = &\quad A_2 \cdot \exp\left\{-\left(\frac{S-<S>_2}{(\Delta S)_2}\right)^2\right\} \end{aligned} \tag{5.57}$$

Both models

$$N\{H\} = \int_H^\infty (n_1\{S\} + n_2\{S\})\mathrm{d}S \tag{5.58}$$

$$V\{H\} = C \cdot (n_1\{H\} + n_2\{H\}) \cdot \left(\frac{1}{N\{H\}}\right)^{\frac{1}{3}} \tag{5.59}$$

5.8 Comparison with experimental data

Models 1 and 2 were tested against experimental data from Moorthy *et al.* (1998) on a 0.22 C 0.12 Mn wt. % steel, quenched and tempered at 600°C

for a range of times between 0.5 and 100 hours (Figure 5.2). These data were chosen because, after the earliest stages of tempering, there was only one type of carbide present: Fe_3C. Also, published data on the average grain and carbide sizes in these steels were available. Data were acquired using the program 'DataThief', which converts images into digital data.

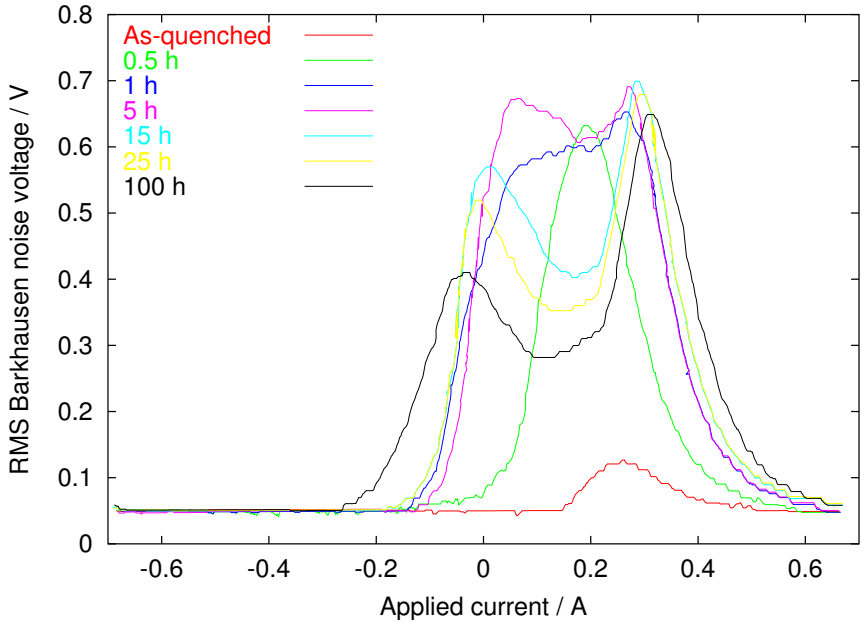

Figure 5.2: Real BN data from tempered 0.22 C 0.12 Mn wt. % steel. Data from Moorthy *et al.*, 1998.

Programs were written to fit Models 1 and 2 to the experimental data. The Fortran 77 code for the Model 2 program, and details of the fitting methodology, are given in the Appendix.

The fitted BN curves are shown in Figure 5.3–Figure 5.8. The horizontal scales on these diagrams are in units of magnetising current rather than applied field, but the field is proportional to the current so the shape of the curve is not affected by this. It can be seen that single peaks can be fitted very well using both models (Figure 5.3). Model 2 is better at fitting shoulder behaviour (Figure 5.4) and two-peak behaviour (Figure 5.8). The region between the peaks is the most problematic for both models; the real

V value is higher than the modelled value, causing the fitted peaks to move closer together than the real peaks. The noise in this central area may be due to pinning by intragranular dislocations, which have not been considered in either model.

The 'error' figure quoted to quantify the goodness of fit is calculated using:

$$E = \left[\frac{\sum(V_r\{H\} - V_p\{H\})^2}{\sum(V_r\{H\})^2}\right]^{-\frac{1}{2}} \cdot 100\% \tag{5.60}$$

where $V_r\{H\}$ is the real value and $V_p\{H\}$ the predicted value of the RMS Barkhausen voltage V at field H.

Barkhausen two-peak data may also be analysed by fitting a normal distribution to each peak. The total amplitude is given by the sum of two expressions of the form of n_1 and n_2 in Equation 5.56 (but since Equation 5.58 and Equation 5.59 are not considered, the parameters in the normal distribution expressions have different meanings from those in Equation 5.56). The error due to fitting using this method was compared with the errors due to the two models. The results in Table 5.1 show that, while the peak-fitting method sometimes produces a fit comparable with that of Model 1, Model 2 performs consistently better, especially at longer tempering times when the double-peak behaviour is well developed.

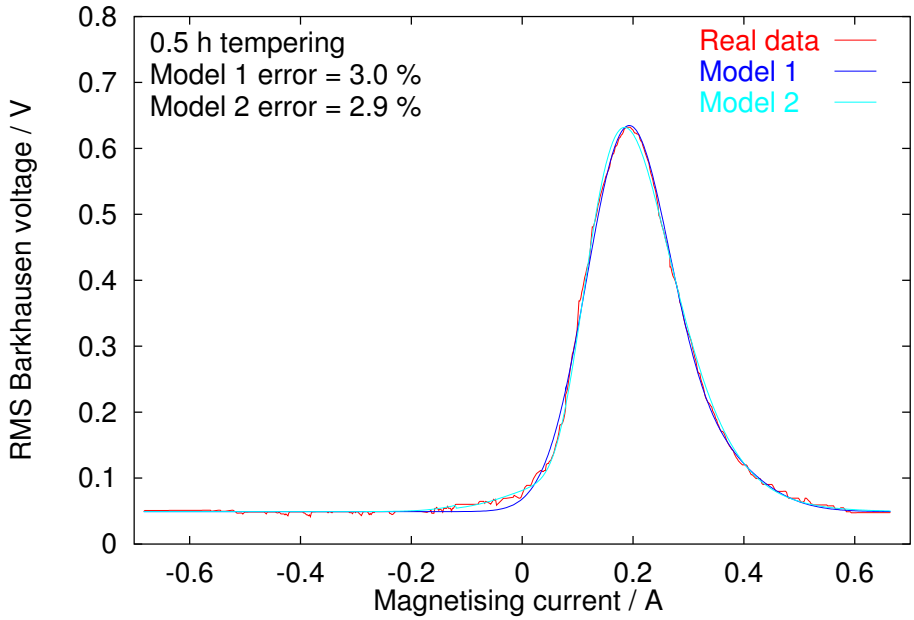

Figure 5.3: Fitting of data for plain-carbon steel tempered for 0.5 h.

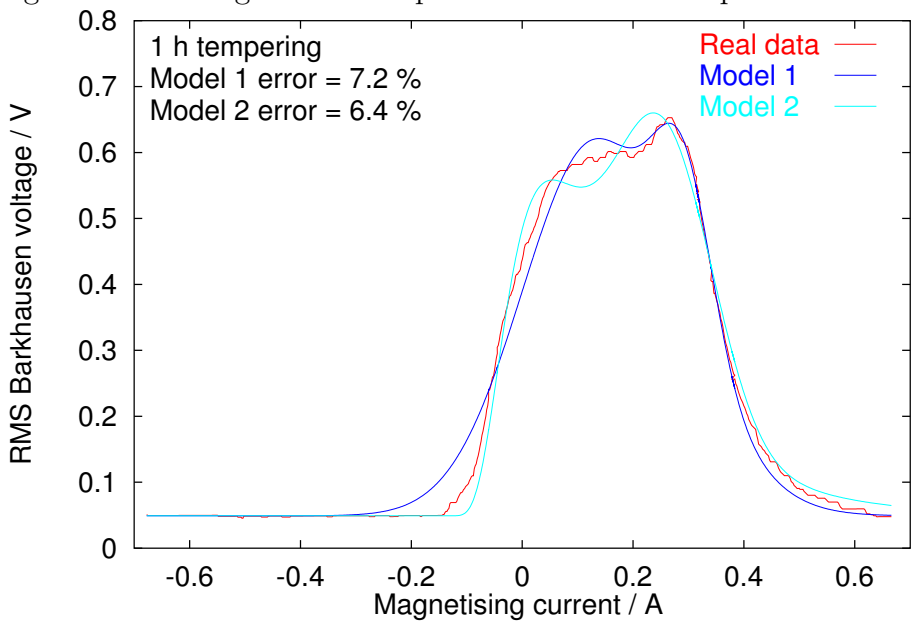

Figure 5.4: Fitting of data for plain-carbon steel tempered for 1 h.

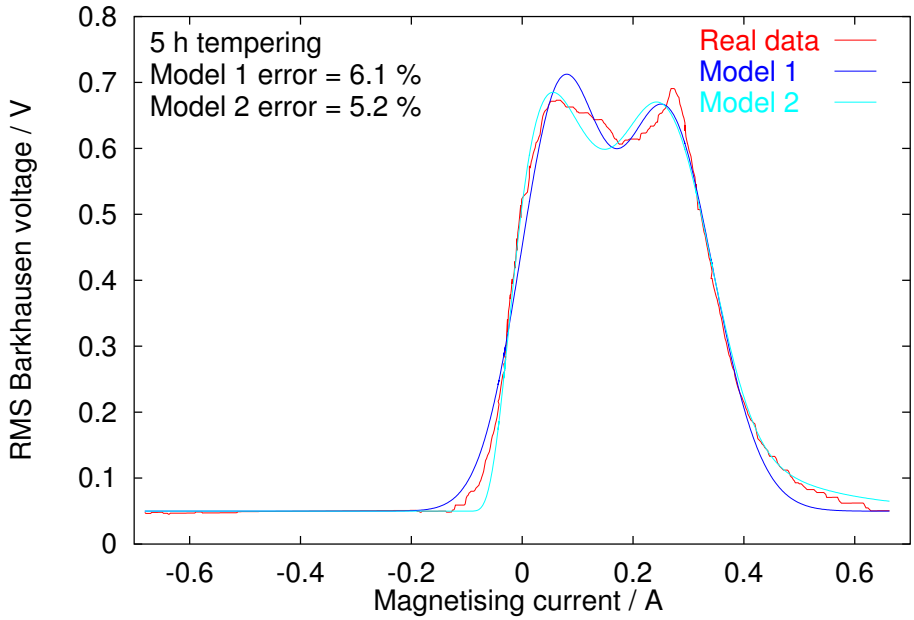

Figure 5.5: Fitting of data for plain-carbon steel tempered for 5 h.

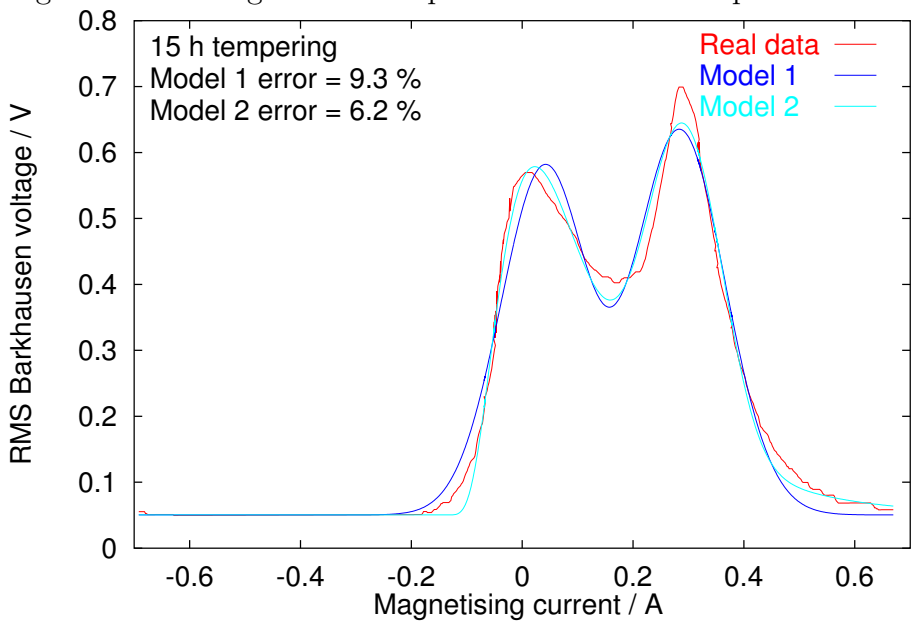

Figure 5.6: Fitting of data for plain-carbon steel tempered for 15 h.

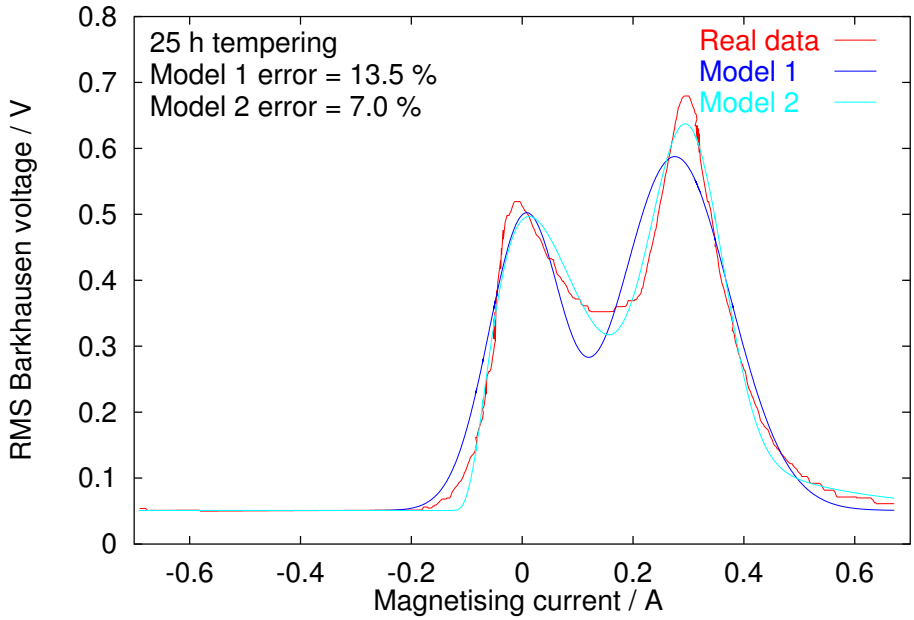

Figure 5.7: Fitting of data for plain-carbon steel tempered for 25 h.

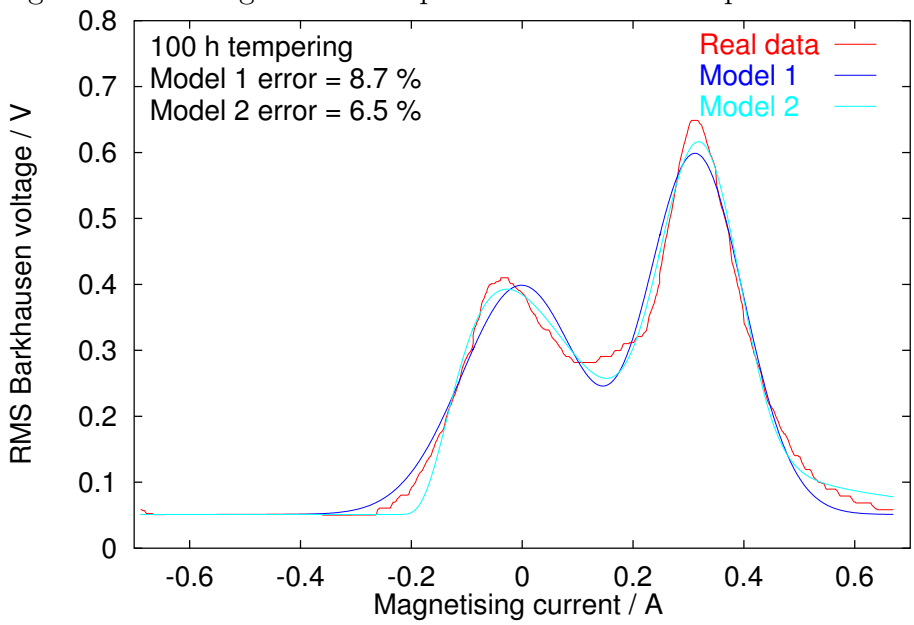

Figure 5.8: Fitting of data for plain-carbon steel tempered for 100 h.

Time	Error (%)		
	Peak-fitting	Model 1	Model 2
0	3.58	3.60	3.14
0.5	2.98	3.03	2.85
1	13.1	7.18	6.44
5	6.16	6.05	5.20
15	9.01	9.31	6.23
25	13.9	13.5	6.96
100	8.44	8.69	6.53
Mean	**8.17**	**7.34**	**5.34**

Table 5.1: Fitting errors of arbitrary peak-fitting, Model 1 and Model 2.

5.9 Relationship between fitting parameters and metallographic data

5.9.1 Pinning strength relationships to grain and carbide sizes

In order to test whether the model has any physical basis, the fitting parameters obtained were compared with grain and carbide size data from the work of Moorthy *et al.*

In Model 1, the parameters $< S >_1$ and $< S >_2$ represent the average pinning strengths of the two distributions. Figure 5.9 shows a decrease in $< S >_1$ with increasing grain size, but an indeterminate relationship between $< S >_2$ and carbide size.

In Model 2, the average pinning strength of the log-normal distribution is given by $e^{<x>} + S_b$ (Equation 5.54). Figure 5.10 shows a clear decrease in $e^{<x>} + S_b$ with increasing grain size, and an increase in $< S >_2$ with increasing carbide size. These trends correspond well with the expected pinning strength behaviour of grain boundaries and carbides in tempered steels. It is therefore likely that Model 2 has a more reliable physical basis than Model 1. Since the relationships between the modelling parameters and the microstructural measurements are approximately linear, it should

Time	Grain size / μm	Carbide size / μm	Fitting error / %
1	3.7	0.13	9.29
5	5.6	0.17	5.63
15	8.9	0.26	8.00
25	10.7	0.34	7.05
100	21.5	0.46	6.82

Table 5.2: Fitting errors for model with values of $e^{<x>} + S_b$ and $< S >_2$ calculated from microstructural data.

be possible to estimate grain and carbide sizes within this range by fitting the Barkhausen profile using this model.

5.9.2 Fitting of model to microstructural data

Linear regression was applied to obtain the slopes of the straight lines on Figure 5.10. Using these slopes, values of $e^{<x>} + S_b$ and $< S >_2$ calculated from the grain and carbide sizes respectively were substituted into the model and the other parameters fitted as before. Table 5.2 shows the errors generated by this fitting. They are larger than those for Model 2 in Table 5.1, but still lower than for peak-fitting, and for Model 1 in all cases but one. As before, the superiority of Model 2 is more evident at longer tempering times.

5.9.3 Tests of the model on other data sets

Three further data sets were available, from a 0.22 C, 0.02 Mn wt. % steel, a $2\frac{1}{4}$Cr1Mo and a 9Cr1Mo steel (Moorthy *et al.*, 1997b, 1998, 2000). Model 2 was fitted to these data sets, and the variation of the fitting parameters with tempering time was studied.

Carbon-manganese steels

Comparisons between the Model 2 fitting parameters from the two C-Mn steel data sets are shown in Figure 5.11–Figure 5.14. Fitting of the 5 hour data set gave a ΔS_2 value several orders of magnitude greater than those of the other data sets. This was clearly an unphysical solution, and an indication

that the fitting program must be modified to avoid even infrequent failures of this sort. This point was removed from the plots so that trends in the other values could be seen. Figure 5.11 shows the variation of $e^{<x>} + S_b$, with tempering time. It initially drops very rapidly, then decreases more slowly at longer times. This corresponds well with the expected changes in grain boundary pinning strength, with an initial rapid decrease as the dislocation density reduces, followed by a more gradual change as coarsening and recrystallisation take place. The peak at 5 hours in the blue curve is from the same set of parameters as the unrealistic ΔS_2 value was found, so the $e^{<x>} + S_b$ value here may also be unreliable.

$< S >_2$ increases rapidly at short tempering times, then begins to level off at longer times (Figure 5.12). This may be due to the pinning site strength increasing as the carbides coarsen, then reaching the critical size for spike domain formation at longer times.

The relationship betwen Δx and the tempering time is less clear (Figure 5.13), but the variation of ΔS_2 with tempering time is consistent between the two steels. However, ΔS_2 does not correspond to the widths of the carbide size distributions published by Moorthy *et al.* (1997b), which increase monotonically with tempering time.

Power plant steels

Figure 5.15 and Figure 5.16 show experimental data from $2\frac{1}{4}$Cr1Mo and 9Cr1Mo steels respectively. The variations of $e^{<x>} + S_b$ and $< S >_2$ with tempering time for these data are plotted in Figure 5.17 ($2\frac{1}{4}$Cr1Mo) and Figure 5.18 (9Cr1Mo). In both cases, $e^{<x>} + S_b$ decreases rapidly in the very early stages of tempering, before increasing slightly at longer times. $< S >_2$ peaks at an intermediate tempering time in the $2\frac{1}{4}$Cr1Mo steel, but not in the 9Cr1Mo steel. This may be related to a real phenomenon involving carbide precipitation sequences, or to errors in fitting. It is difficult to know which is the case without carbide size data for these steels.

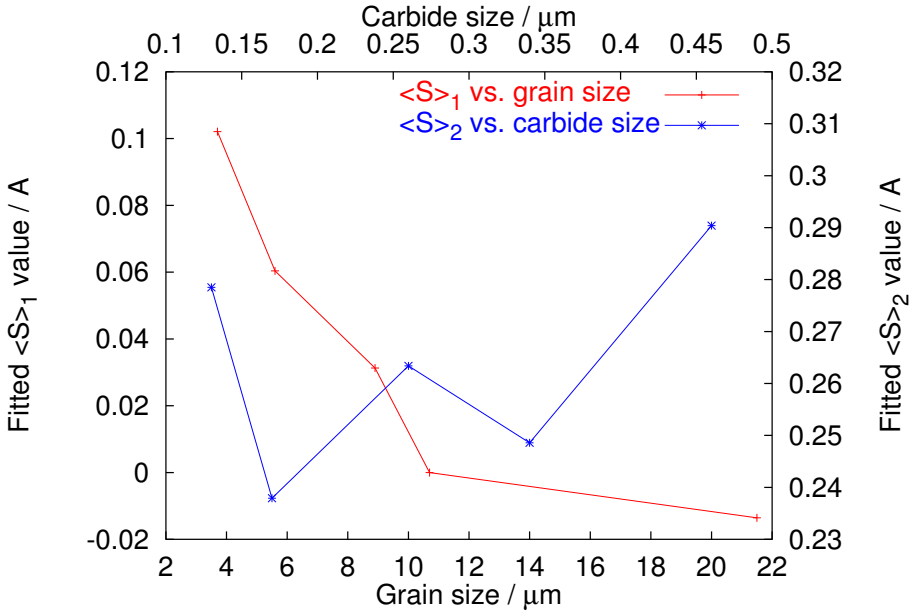

Figure 5.9: Fitting parameters $< S >_1$ versus grain size and $< S >_2$ versus carbide size for Model 1.

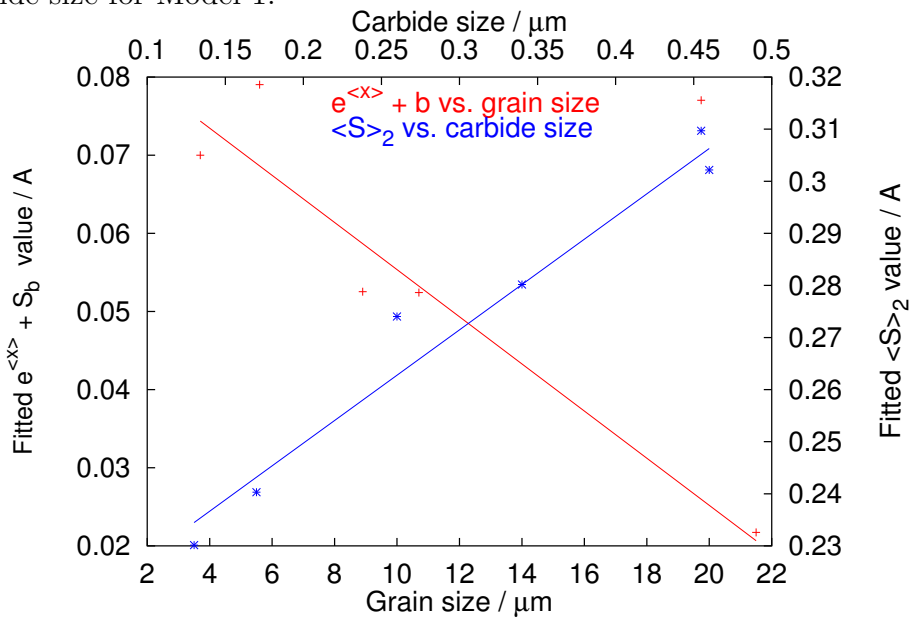

Figure 5.10: Fitting parameters $e^{<x>} + S_b$ versus grain size and $< S >_2$ versus carbide size for Model 2.

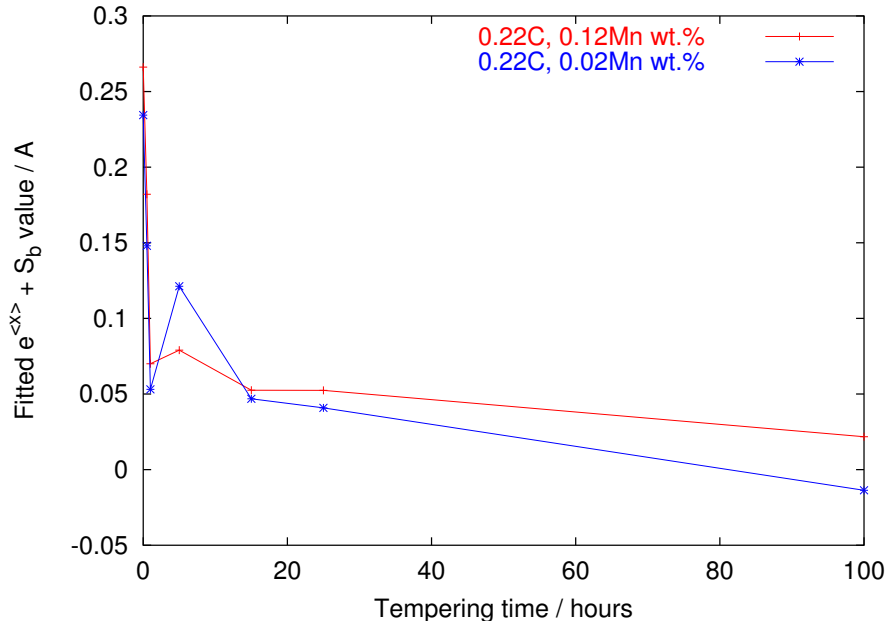

Figure 5.11: Relationship of Model 2 fitting parameters $e^{<x>} + S_b$ with tempering time for two steels of similar composition.

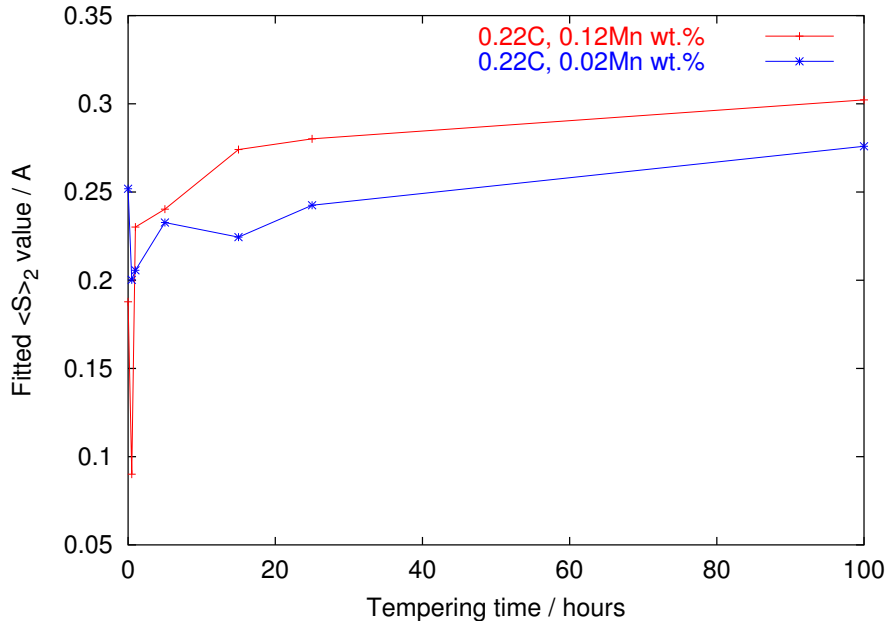

Figure 5.12: Relationship of Model 2 fitting parameter $< S >_2$ with tempering time for two steels of similar composition.

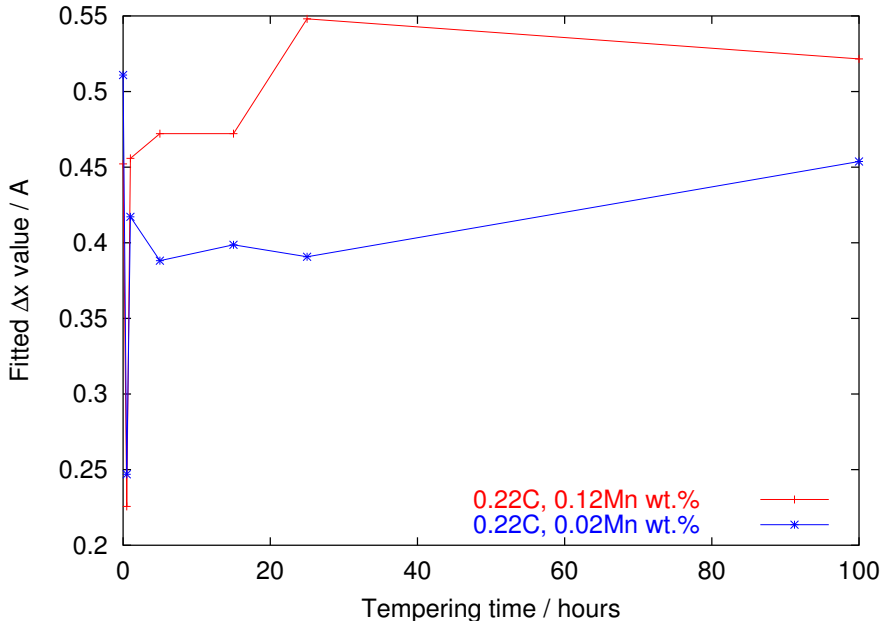

Figure 5.13: Relationship of Model 2 fitting parameter Δx with tempering time for two steels of similar composition.

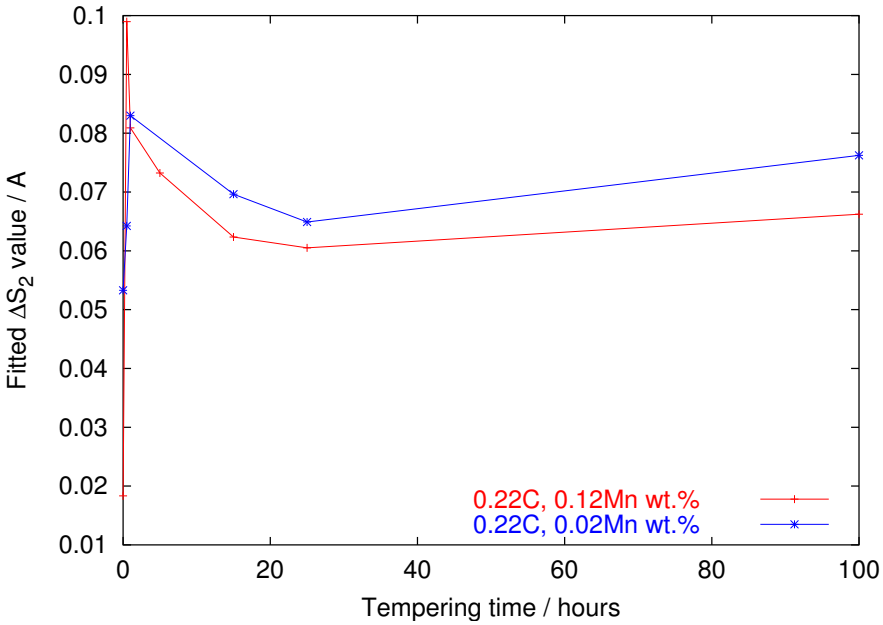

Figure 5.14: Relationship of Model 2 fitting parameters ΔS_2 with tempering time for two steels of similar composition.

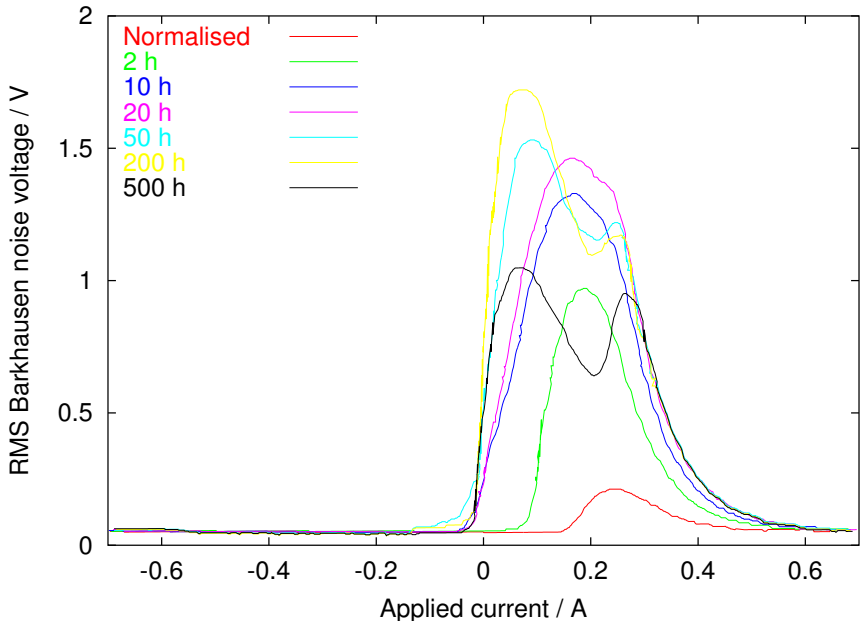

Figure 5.15: Real BN data from tempered $2\frac{1}{4}$Cr1Mo power plant steel. Data from Moorthy *et al.*, 1998.

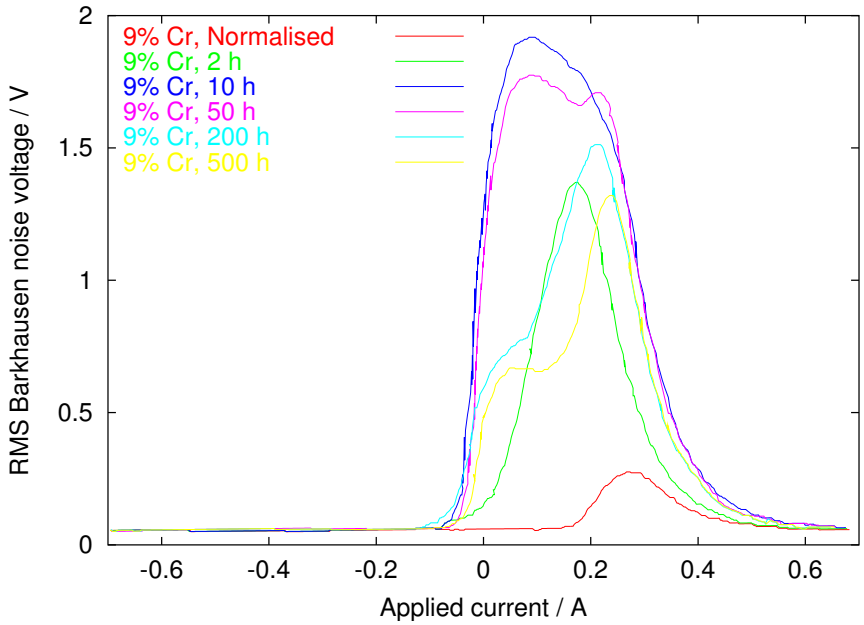

Figure 5.16: Real BN data from tempered 9Cr1Mo power plant steel. Data from Moorthy *et al.*, 1998.

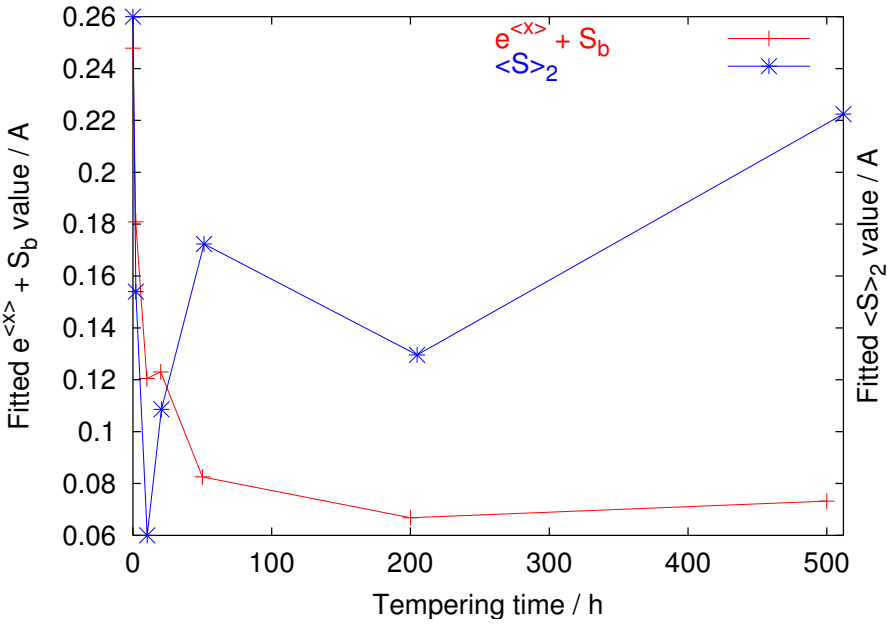

Figure 5.17: Model 2 fitting parameters $e^{<x>} + S_b$ and $< S >_2$ versus time for $2\frac{1}{4}$Cr1Mo steel.

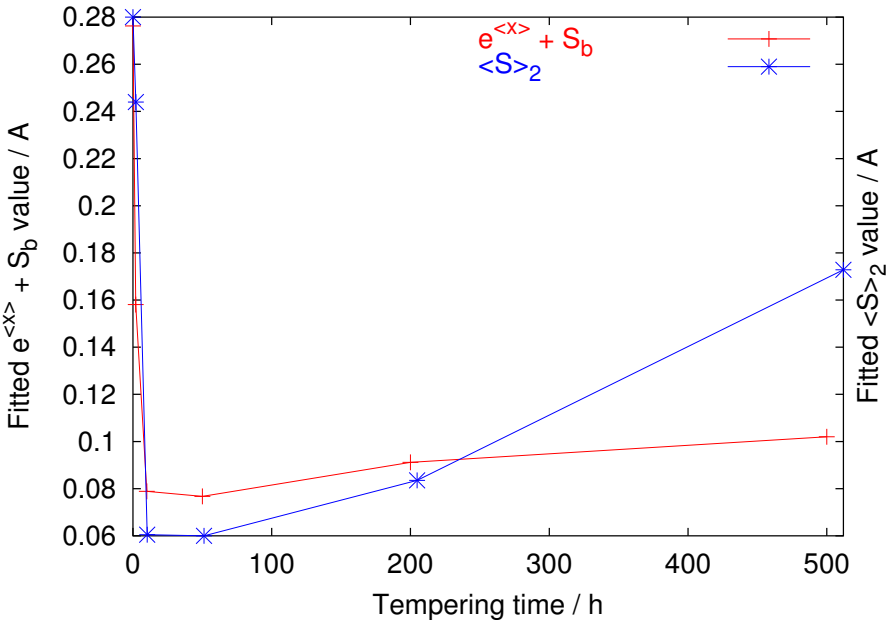

Figure 5.18: Model 2 fitting parameters $e^{<x>} + S_b$ and $< S >_2$ versus time for 9Cr1Mo steel.

5.10 Discussion

Model 2 fits experimental data well in most cases, and it is therefore likely that its physical basis is better than that of Model 1. In order to test the model further and to understand the relationships of its modelling parameters with microstructural data, it is necessary to obtain BN data sets from a wide range of samples with well characterised microstructures. The following four chapters describe the microstructural characterisation, BN experiments and model-fitting carried out for this purpose.

It appears that, despite extensive testing before use, the fitting program cannot always be relied upon to produce reliable parameters. It may be useful to modify the program to limit the range in which the solutions can lie, or to apply other constraints on the basis of experience. Δx and ΔS seem to be the parameters presenting the greatest problems for fitting, possibly because both A and ΔS affect the peak heights, so that it is difficult to determine correctly the effect of these two parameters on a peak.

5.11 Conclusion

Two models have been proposed to interpret BN data obtained from tempered steel. A model using a log-normal distribution of pinning site strengths for the lower-field peak, and a normal distribution for the higher-field peak, gave good agreement with real data. Clear relationships were found between the fitting parameters characterising the centres of the distributions, and measured grain and carbide dimensions. It therefore appears that this model both supports the interpretation of Moorthy *et al.* that two-peak BN signals are due to the separate effects of pinning by grain boundaries and carbides, and provides a basis for microstructural estimation from Barkhausen data. However, it will be necessary to test the model against more experimental data to confirm this relationship, and to improve the fitting method so that it always produces physically realistic model parameters.